

ARTICLE

Numerical and analytical modeling of SPH-ECC strengthened RC beams

M. Qasim¹ | Y. X. Zhang² | C. K. Lee¹ 

¹School of Engineering and Technology,
University of New South Wales, Canberra,
New South Wales, Australia

²School of Engineering, Design and Built
Environment, Urban Transformations
Research Centre, Western Sydney
University, Penrith, New South Wales,
Australia

Correspondence

C. K. Lee, School of Engineering and
Technology, University of New South
Wales, Canberra, 2600 New South Wales,
Australia.

Email: c.lee@adfa.edu.au

Abstract

Many studies have suggested that engineered cementitious composite (ECC) could be a highly efficient and cost-effective material for enhancing the flexural strength of reinforced concrete (RC) beams. Recently two effective retrofitting configurations using steel and polyvinyl-alcohol hybrid fiber reinforced engineered cementitious composite (SPH-ECC) were proposed (Qasim et al., *Eng Struct*, 2023, 284, p. 115992) and their high effectiveness for enhancing the flexural strength of RC beam was verified experimentally. However, to examine the performance of these strengthening configurations thoroughly by conducting experiments to cover practical ranges of design parameters is deemed to be too expensive and time consuming. In this study, a numerical parametric study of SPH-ECC strengthened RC beams was conducted by employing a validated finite element (FE) modeling procedure developed by the authors. The effects of four key design parameters including the compressive strength of concrete and SPH-ECC, the thickness of SPH-ECC strengthening layer and the area of reinforcement bars embedded in SPH-ECC layers on the flexural performance of the strengthened beams were studied. Parametric study results showed that the area of reinforcement bars in the SPH-ECC layers could significantly affect the flexural strength of the strengthened beams. Furthermore, in order to allow engineers to predict the flexural strength of the strengthened beams quickly, two simple but accurate analytical models were also developed for the two strengthening configurations considered. Their reliability and accuracy were then verified and confirmed by comparing with the parametric study results.

KEYWORDS

analytical model, engineered cementitious composite (ECC), flexural strengthening, hybrid fiber, numerical parametric study

This is an open access article under the terms of the [Creative Commons Attribution-NonCommercial-NoDerivs](https://creativecommons.org/licenses/by-nc-nd/4.0/) License, which permits use and distribution in any medium, provided the original work is properly cited, the use is non-commercial and no modifications or adaptations are made.

© 2023 The Authors. *Structural Concrete* published by John Wiley & Sons Ltd on behalf of International Federation for Structural Concrete.

1 | INTRODUCTION

Recently, the use of high performance engineered cementitious composite (ECC) is getting much attention for strengthening of reinforced concrete (RC) structures.^{1,2} High performance ECCs may attain a tensile strain of more than 3% while maintain the crack width below 100 μm .³ Several studies on the application of mono-fiber reinforced ECC such as polyvinyl-alcohol engineered cementitious composite (PVA-ECC) for strengthening RC beams have been reported.^{4,5} It was observed that although PVA-ECC has considerable ductility, it has a relatively low ultimate strength and lower fire resistance.⁶ Lai et al.⁷ reported the use of PE-ECC in their experimental study on the axial compressive behavior of steel RC columns with stay in place ECC jackets. It was found that while the stay in place ECC jacket displayed a lower stiffness, it improved the deformation capacity and enhanced confinement effect. In addition, ECC jacketing has also been applied to RC short columns and shear-deficient RC members for performance enhancement.^{8,9} Furthermore, PVA-ECC has also been used together with carbon fiber-reinforced polymer (CFRP) grid for flexural strengthening of RC beams.¹⁰ In comparison to mono-fiber ECC such as PVA-ECC, ECCs with both steel and polymer fiber such as steel and PVA fiber reinforced engineered cementitious composite (SPH-ECC) may show a higher ultimate strength and fire resistance while maintains a reasonably high tensile strain capacity. Furthermore, a previous study also shown that SPH-ECC has a good interfacial bond strength with concrete¹¹ so it could has high potential for strengthening existing RC structures.

Tinoco and Silva¹² used SPH-ECC for strengthening RC beams. It was observed that the use of SPH-ECC without any embedded reinforcement cannot significantly enhance the flexural strength of RC beams. Qasim et al. studied the use of SPH-ECC with embedded reinforcement bars for strengthening RC beams¹ and three different types of strengthening configurations were considered. These included (i) strengthening with bottom SPH-ECC layer only (the SB-1 configuration), (ii) strengthening with side SPH-ECC layers only (the SB-2 configuration), and (iii) strengthening with both sides and bottom SPH-ECC layers (the SB-3 configuration). It was found that the SB-1 configuration eventually resulted in premature failure due to interfacial debonding between SPH-ECC and concrete. However, the SB-2 and SB-3 configurations could significantly enhance the flexural strength of beams without premature debonding failure before the ultimate flexural failure state of the strengthened beam was reached.

From the experimental results obtained in Reference 1, it is expected the flexural response of SPH-ECC strengthened RC beam¹³ shall generally depend on the

material properties of the concrete beam and the strengthening materials (i.e., SPH-ECC) as well as the geometric properties of the strength configuration. However, due to resource limitation and time constraint, it is very difficult to perform experimental study to cover all practical ranges of those key design parameters. Therefore, the less costly and less time demanding finite element (FE) modeling technique is often adopted which is very effective and highly efficient for conducting a thorough numerical parametric study¹⁴ to gain more insights on the effects of different key parameters of the strengthening scheme. Toward this end, in the study by Qasim et al.,¹ reliable FE models for strengthened RC beams for the SB-2 and SB-3 strengthening configurations were developed and were validated by comparing the model results with the test results.

While in Reference 1, it was demonstrated that the two strengthening configurations (SB-2 and SB-3) proposed could provide significant enhancements on both the initial stiffness and flexural strength of the original RC beam, a more detailed study on the effects of different design parameter is still required to obtain more useful insights and data on the general behaviors of the strengthened beams. As testing of full-scale beams is deemed to be very time consuming and expensive, the main aim of this study is to investigate the effects of those key design parameters that may affect the flexural strength of SPH-ECC strengthened RC beams by conducting a numerical parametric study. In particular, the parametric investigation was carried out by considering four key design parameters, namely (i) concrete compressive strength of the original RC beam, (ii) compressive strength of SPH-ECC, (iii) thickness of SPH-ECC layers used, and (iv) area of reinforcement bars embedded in the SPH-ECC layers. This proposed numerical parametric study should provide some very important information and insights which are crucial to practical design and could not be obtained from experimental study alone. Furthermore, while FE modeling could produce the detailed load-deflection curve for the strengthened beams, it could still be too complicated for day-to-day design tasks. Hence, by using the invaluable modeling results obtained from the parametric study, two simple analytical models for the SB-2 and SB-3 strengthening configurations were also proposed to predict the flexural strength of the strengthened beams. The accuracy and reliability of these analytical models will then be validated by comparing their predictions against the numerical parametric study results. These analytical models would then allow structural engineers to estimate the flexural strength of the strengthened beams quickly and would be an invaluable tool for the design of the strengthened beams.

2 | THE STRENGTHENED BEAMS CONFIGURATIONS AND FE MODELING PROCEDURE

2.1 | The strengthened schemes

The longitudinal section, reinforcement details, support conditions and loading conditions of the 3.5 m long control beam (i.e., no strengthening) tested in Reference 1 is shown in Figure 1. The cross-sectional details of the control beam together with the SB-2 and SB-3 strengthening configurations are shown in Figure 2.¹ As shown in Figure 2, the SB-2 strengthening configuration was obtained by adding SPH-ECC layers and additional reinforcement bars at the two sides of the control beam. While for the SB-3 configuration, SPH-ECC layers were attached at both the bottom and the two sides of the control beam with reinforcement bars embedded in the bottom SPH-ECC layer. In order to ensure a ductile failure mode (i.e., yielding of reinforcement bars before crushing of concrete/ECC layers), all strengthened beams were designed to be still under-reinforced after strengthening. For the selection of rebar size, it was largely depended on the practical size constraints for the strengthened beam. In particular, due to headroom constraint and width constraint in practical applications, it is unlikely that

the width and depth of the strengthened beam could be more than 20% and 33% of the original beam, respectively. Hence, the thickness of the SPH-ECC layer of the tested beams used was limited to 50 mm. The rebar diameter used was 16 mm due to minimum cover requirement. For the arrangement of the rebar, it is obviously better to place them symmetrically and close to the bottom of the beam in order to increase the flexural strength of the beam.¹

It should be mentioned that in the actual tests,¹ no special treatment (e.g., sandblasting) was employed to roughen the concrete surface before the SPH-ECC layers were applied. That is, all concrete surfaces can be considered as under an “As-cast” condition. This decision was based on the reasons that (i) in a previous study,¹¹ it was found that sufficient bond strength was observed between concrete and SPH-ECC interface and (ii) in practice, using as-cast surface without any surface treatment could reduce the cost of the retrofitting procedure.

2.2 | FE model used in the numerical parametric study

Typical FE model of the strengthened beam for the SB-3 configuration is shown in Figure 3.¹ In Figure 3, a mesh

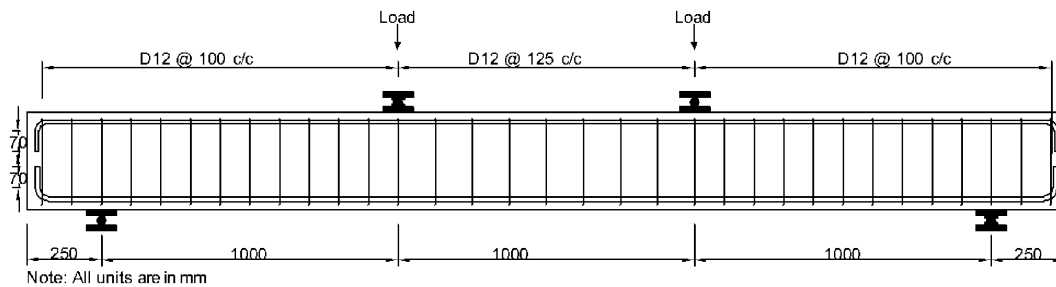


FIGURE 1 Longitudinal section of control RC beam and loading and support conditions. All units are in mm; D = diameter of reinforcement bar.

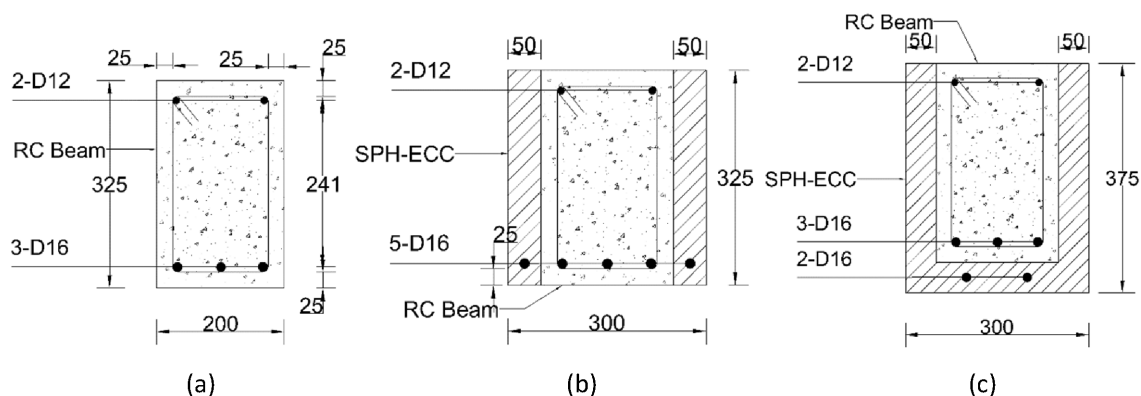


FIGURE 2 Cross-sectional details of beams tested in Reference 1: (a) control beam; (b) SB-2 strengthened configuration; and (c) SB-3 strengthened configuration.

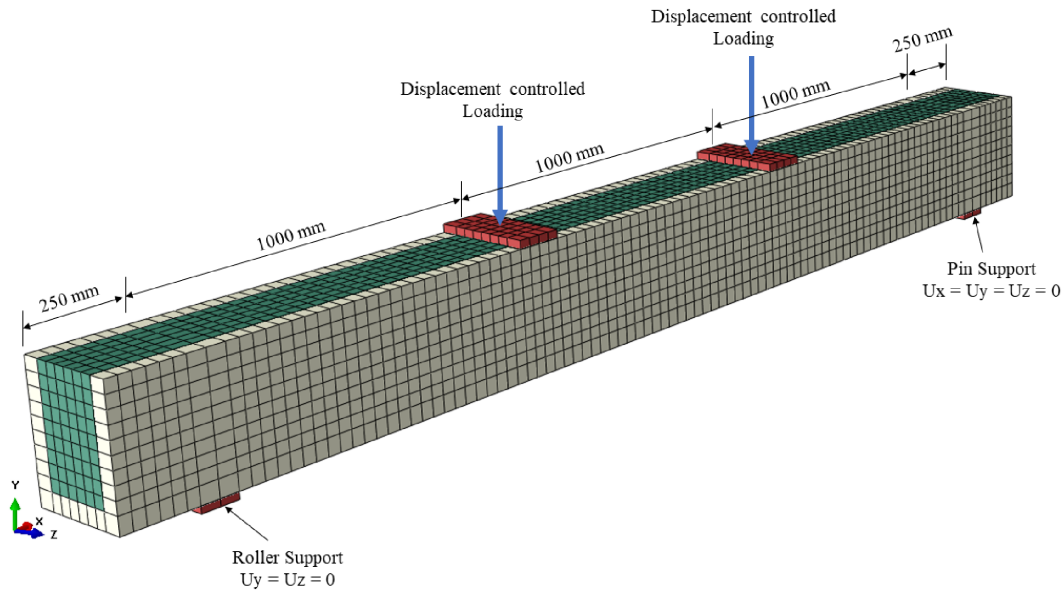


FIGURE 3 Typical finite element model of beam strengthened with SB-3 configuration.

size of 35 mm was used and it was based on the mesh sensitivity analysis results.¹ The same boundary conditions used in the actual tests were applied in the model. Note that the FE model for strengthened beam with SB-2 configuration is very similar to that of SB-3 model with the only difference of the absent of ECC layer at the bottom part of the beam. It should be noted that in Reference 1, in order to study the interfacial bond slip behavior between the concrete and ECC surfaces, computational expensive surface-to-surface cohesive elements were inserted at all SPH-ECC-to-concrete interfaces during the FE analysis. However, from the test results, it was observed that for both SB-2 and SB-3 configurations, even all SPH-ECC layers were applied under the as-cast condition without any surface roughening treatment, no interfacial debonding between SPH-ECC and concrete was observed before ultimate failure. Therefore, for all FE models used in the numerical parametric study, in order to reduce the computational resource needed, the simpler and less computational demanding tie constraint was used in lieu of the cohesive elements at all SPH-ECC-to-concrete interfaces^{13–15} (A FE analysis using the cohesive elements required at least 400% more computational time to complete.). The FE analysis package ABAQUS¹⁶ was employed as the modeling platform. Reinforcement bars used in the RC beam part and the SPH-ECC layers were modeled using truss elements with embedded region constraint¹³ as no bond slip between the reinforcement bars and the concrete/SPH-ECC was observed in the tests. The SPH-ECC and concrete components of the beams were modeled using eight-node solid brick element (C3D8R).

TABLE 1 Concrete Damage Plasticity (CDP) model parameters for concrete and SPH-ECC.

ψ	ϵ	f_{b0}/f_{c0}	K_C	μ_V
36°	0.1	1.16	0.667	0.001

2.3 | Constitutive material models used in the parametric study

In order to obtain reliable predictions of the behaviors of the strengthened beams until failure, sound and realistic constitutive material models for steel reinforcement bars, concrete and SPH-ECC are essential.

2.3.1 | Constitutive model for reinforcement bars and concrete

The constitutive model for reinforcement bars was defined by using a simple bilinear plastic model based on the direct tensile coupon test results obtained in Reference 1. The yield and ultimate strengths of the reinforcement bars are 590 MPa and 680 MPa, respectively.

The concrete damaged plasticity (CDP) model available in ABAQUS¹⁶ was employed to describe the damage evolutions of concrete. The CDP model is a well-proved reliable model to simulate both compressive and tensile behavior of cementitious materials such as concrete and SPH-ECC.¹³ It requires five key parameters which are listed in Table 1. These parameters are (i) the dilation angle (ψ), (ii) the flow potential eccentricity (ϵ), (iii) the ratio of the compressive strength under biaxial loading

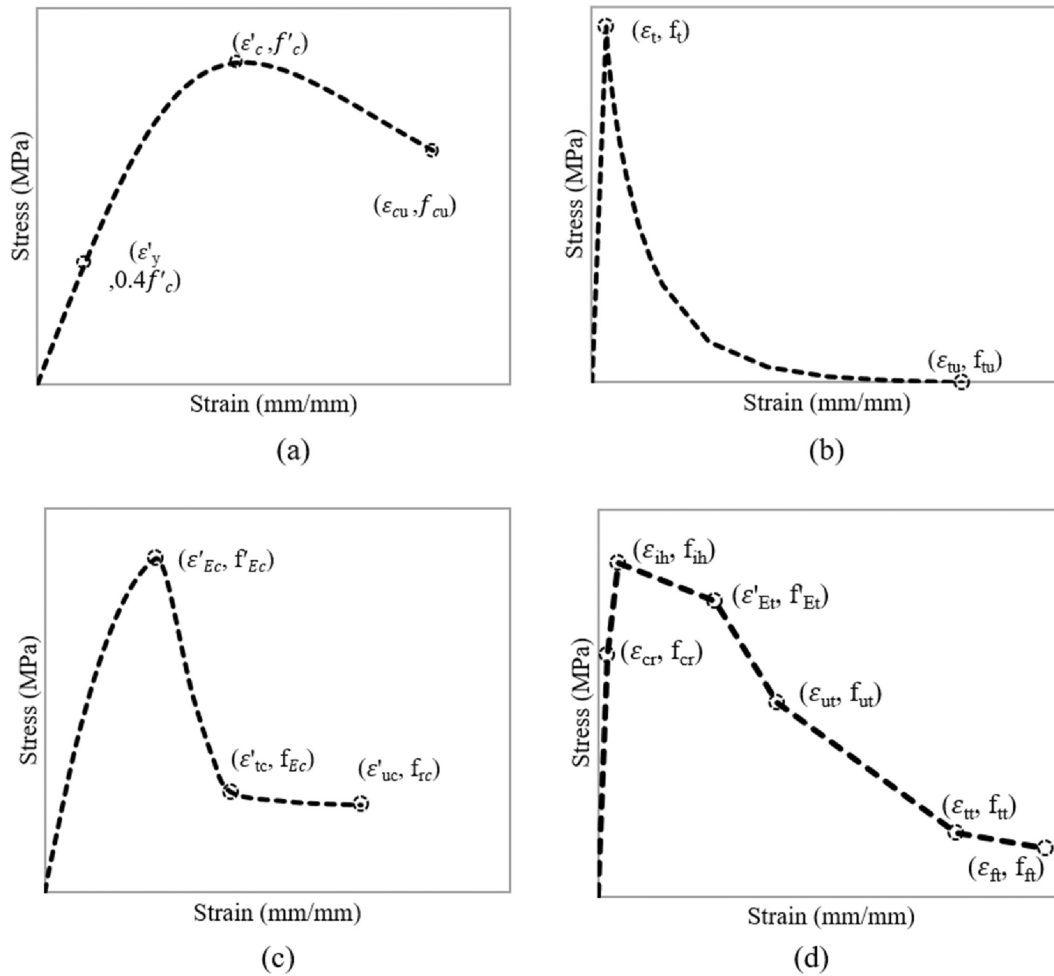


FIGURE 4 Stress–strain relationship for concrete under (a) uniaxial compression (b) uniaxial tension and for SPH-ECC under (c) uniaxial compression (d) uniaxial tension.

(f_{bo}) to uniaxial compressive strength (f_{co}), (iv) the ratio of the second stress invariant on the tensile meridian to that on the compressive meridian (K_C), and (v) the viscosity parameter (μ_v). It should be noted that values in Table 1 were selected based on previous relevant research.¹⁷

For the compressive constitutive model of concrete, the model proposed by Carrier and Chu¹⁸ (Figure 4a) was employed:

$$f_c = f'_c \left[\frac{\beta \left(\frac{\epsilon}{\epsilon'_c} \right)}{\beta - 1 + \left(\frac{\epsilon}{\epsilon'_c} \right)^\beta} \right] \quad (1a)$$

where

$$\beta = \left| \frac{f_{tc}}{32.4} \right|^3 + 1.55 \quad (1b)$$

In Equation (1), f'_c and ϵ'_c is the peak compressive strength and the corresponding strain, respectively. Their

values can be obtained from standard compressive test easily. The tensile behavior of concrete was defined by the constitutive model proposed by Hassan¹⁹ (Equation 2 and Figure 4b).

$$f_t = \begin{cases} \epsilon E_c & 0 < \epsilon \leq \epsilon'_{tc} \\ f'_{tc} \exp \left[- \left(\frac{\epsilon - \epsilon'_{tc}}{\alpha_1} \right)^{\beta_1} \right] & \epsilon'_{tc} < \epsilon \leq \epsilon_{tu} \end{cases} \quad (2a)$$

where

$$\epsilon_{tu} = 25\epsilon'_{tc}, \alpha_1 = 0.00035, \beta_1 = 0.85 \quad (2b)$$

In Equation (2), f'_{tc} is the peak tensile stress of concrete (through indirect tensile tests). $\epsilon'_{tc} = f'_{tc}/E_c$ is the corresponding strain of f'_{tc} . E_c is the elastic modulus of concrete. It should be noted that the stress–strain parameters used in Equation (2) are depended on the compressive strength (f'_c) of the concrete. In the following numerical parametric study (Section 3), two different

TABLE 2 Values of stress–strain model parameters for concrete with $f'_c = 30$ MPa.

Compression				Tension			
Strain	Stress		Strain	Stress		Strain	Stress
ϵ_c	0.1	$0.4f'_c$	12.0	ϵ_t	0.01	f_t	3.0
ϵ_o	0.33	f'_c	30.0	ϵ_{tu}	0.25	f_{tu}	0
ϵ_{ou}	0.7	f_{cu}	24.4	-	-	-	-

Note: Strain is in percentage; stress is in MPa.

values of $f'_c = 30$ MPa and $f'_c = 45$ MPa were used. Values of these stress–strain parameters for concrete with $f'_c = 30$ MPa and $f'_c = 45$ MPa are listed in Tables 2 and 3, respectively.

2.3.2 | Constitutive model for SPH-ECC

For the damage mode of SPH-ECC, again the same CDP model was used with the same parametric values shown in Table 1. For SPH-ECC under compression, the constitutive model proposed by Khan et al.¹⁴ was used and is defined by Equation (3) and Figure 4c.

$$f_{Ec} = \begin{cases} f'_{Ec} \left[\frac{\epsilon}{\epsilon'_{Ec}} \left\{ 0.8 \left(1 - \frac{\epsilon}{\epsilon'_{Ec}} \right) + 1 \right\} \right] & 0 \leq \epsilon \leq \epsilon'_{Ec} \\ f'_{Ec} \left[\frac{n(\epsilon/\epsilon'_{Ec})}{1 + (n-2) \left(\frac{\epsilon}{\epsilon'_{Ec}} \right) + (\epsilon/\epsilon'_{Ec})^2} \right] + f'_{rc} & \epsilon'_{Ec} < \epsilon \leq \epsilon'_{uc} \end{cases} \quad (3)$$

In Equation (3), f'_{Ec} and ϵ'_{Ec} are the peak compressive stress and corresponding strain of SPH-ECC, respectively. ϵ'_{uc} is the ultimate compressive strain. n is a controlling parameter defining the shape of the post peak softening curve (Equation 4).

$$n = -f'_{rc} \left[\frac{\epsilon'_{Ec}{}^2 - 2\epsilon'_{Ec}\epsilon'_{tc} + \epsilon'_{tc}{}^2}{\epsilon'_{Ec}\epsilon'_{tc}(f'_{rc} - f'_{Ec})} \right] \quad (4)$$

In Equation (4), ϵ'_{tc} is the transition point strain in the post peak phase. f'_{rc} is the residual strength which can be expressed as

$$f'_{rc} = f'_{Ec} \left(3.1(f'_{Ec})^{-0.55} \right) \quad (5)$$

The multilinear constitutive model as proposed by Khan et al.¹⁴ (Figure 4d) was adopted for the stress–strain

TABLE 3 Values of stress–strain model parameters for concrete with $f'_c = 45$ MPa.

Compression				Tension			
Strain	Stress		Strain	Stress		Strain	Stress
ϵ_c	0.06	$0.4f'_c$	17.6	ϵ_t	0.01	f_t	3.6
ϵ_o	0.34	f'_c	45.0	ϵ_{tu}	0.25	f_{tu}	0
ϵ_{ou}	0.7	f_{cu}	39.3	-	-	-	-

Note: Strain is in percentage; stress is in MPa.

relationship of SPH-ECC under tension and is defined by Equation (6).

$$f_{Et} = \begin{cases} \frac{f_{cr}\epsilon}{\epsilon_{cr}} & 0 \leq \epsilon \leq \epsilon_{cr} \\ f_{cr} + (f_{ih} - f_{cr}) \left(\frac{\epsilon - \epsilon_{cr}}{\epsilon_{ih} - \epsilon_{cr}} \right) & \epsilon_{cr} \leq \epsilon \leq \epsilon_{ih} \\ f_{ih} + (f'_{Et} - f_{ih}) \left(\frac{\epsilon - \epsilon_{ih}}{\epsilon'_{Et} - \epsilon_{ih}} \right) & \epsilon_{ih} \leq \epsilon \leq \epsilon'_{Et} \\ f'_{Et} + (f_{ut} - f'_{Et}) \left(\frac{\epsilon - \epsilon'_{Et}}{\epsilon_{ut} - \epsilon'_{Et}} \right) & \epsilon'_{Et} \leq \epsilon \leq \epsilon_{ut} \\ f_{ut} + (f_{tt} - f_{ut}) \left(\frac{\epsilon - \epsilon_{ut}}{\epsilon_{tt} - \epsilon_{ut}} \right) & \epsilon_{ut} \leq \epsilon \leq \epsilon_{tt} \\ f_{tt} + (f_{ft} - f_{tt}) \left(\frac{\epsilon - \epsilon_{tt}}{\epsilon_{ft} - \epsilon_{tt}} \right) & \epsilon_{tt} \leq \epsilon \leq \epsilon_{ft} \end{cases} \quad (6)$$

In Equation (6), f_{cr} and ϵ_{cr} are the first cracking stress and corresponding strain, respectively. f_{ih} and ϵ_{ih} are the peak tensile stress and corresponding strain, respectively. f'_{Et} and ϵ'_{Et} are the tensile stress and strain at the point where the SPH-ECC tensile strength a significant drop with crack localization. f_{ut} and ϵ_{ut} are the ultimate limit point of stress–strain curve. f_{tt} and ϵ_{tt} represent the point where softening transition phase starts to be stabilized. Lastly, f_{ft} and ϵ_{ft} define to the failure point.

Similar to the compressive and tensile properties of concrete, values of those parameters used in Equation (6) are generally depended on the compressive strength of ECC (f'_{Ec}). That is, when designing the SPH-ECC mix, one cannot vary these characteristics values independently without changing the compressive strength and vice visa. It should be noted that in the experimental study by Qasim,¹¹ SPH-ECC with compressive strength of 70 and 75 MPa were used in the tests for the SB-2 and SB-3 beams, respectively. In the numerical parametric study (Section 3), an additional value of $f'_{Ec} = 50$ MPa was considered. Hence, three different values of $f'_{Ec} = 50, 70$ and 75 MPa were used in the numerical parametric study. Values of parameters used in Equation (6) for $f'_{Ec} = 50, 70$ and 75 MPa are listed in Tables 4 and 5 for SPH-ECC under compression and tension, respectively.

TABLE 4 Values of stress–strain model parameters for SPH-ECC under compression.

Compressive strength of SPH-ECC (MPa)	ϵ'_{Ec}	f'_{Ec}	ϵ'_{tc}	f_{Ec}	ϵ'_{uc}	f_{rc}
50	0.52	50.0	0.75	25	2.5	20.3
70	0.56	70.0	0.84	35.0	2.8	20.9
75	0.59	75.0	0.89	37.5	2.9	21.6

Note: Strain is in percentage; stress is in MPa.

TABLE 5 Values of stress–strain model parameters for SPH-ECC under tension.

Compressive strength of SPH-ECC (MPa)	ϵ_{cr}	f_{cr}	ϵ_{ih}	f_{ih}	ϵ'_{Et}	f_{Et}	ϵ_{ut}	f_{ut}	ϵ_{tt}	f_{tt}	ϵ_{ft}	f_{ft}
50	0.03	5.0	0.07	6.0	0.63	5.0	0.85	2.6	1.7	1.0	2.3	0.7
70	0.01	5.7	0.06	6.7	0.4	6.4	0.58	5.0	1.0	3.0	2.5	1.5
75	0.05	5.0	0.11	6.9	0.65	6.5	1.0	4.0	2.0	1.3	2.5	1.0

Note: Strain is in percentage; stress is in MPa.

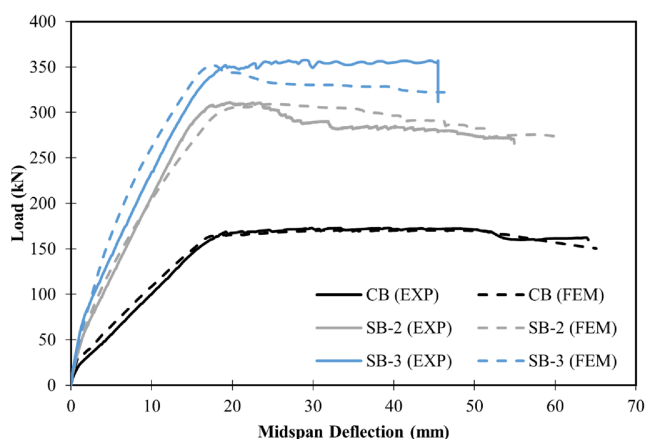


FIGURE 5 Comparison of experimental and FE modeling results of control beam, SB-2 strengthening configuration, and SB-3 strengthening configuration.

2.4 | Verification of the FE model

In order to verify the FE models for the control beam and the strengthened beams with tie constraint applied at SPH-ECC-to-concrete surface interfaces, the load–deflection responses of FE models were compared with their respective experimental load–deflection curves obtained by four-point bending tests¹ in Figure 5. In addition, the maximum load carrying capacities obtained from the FE models were compared to the experimental results in Table 6. It can be concluded from Figure 5 and Table 6 that the FE models developed could accurately predict the flexural responses of both the control beam and strengthened beams until the beams failed. In addition to the load–deflection curves, detailed analysis of the modeling results¹ also showed that the FE model could also capture the failure modes (crushing of top concrete/SPH-ECC layers after yielding of the reinforcement bars in the SPH-ECC layers), the cracking pattern, the strain

distribution of SPH-ECC and the detailed bond slip histories after the ultimate of strength of the beams for both configurations. Therefore, it can be concluded that the FE modeling approach used is accurate, reliable and suitable for conducting the numerical parametric study.

3 | NUMERICAL PARAMETRIC STUDY AND RESULTS

3.1 | Design of the numerical parametric study

In the numerical parametric study, the validated FE models are employed for investigating flexural responses of SPH-ECC strengthened beams with different material and geometric properties and the results obtained will be employed to develop analytical models for day-to-day design of such strengthened beams. In particular, from the test results in Reference 1, it was identified that the flexural strength of the strengthened beams could be affected by (i) the concrete compressive strength of the RC beam, (ii) the SPH-ECC compressive strength, (iii) the SPH-ECC layer thickness, and (iv) the area of reinforcement bars embedded in SPH-ECC layers. Therefore, a number of different FE models were created in the numerical parametric study to investigate the effects of these four key properties. In order to study the effect of concrete compressive strength, two different concrete compressive strengths of 30 MPa and 45 MPa were used. For compressive strengths of SPH-ECCs, two different values of 50 MPa and 70 MPa were used for models with SB-2 configuration while two values of 50 MPa and 75 MPa were used for models with SB-3 configuration.

It should be mentioned that while the compressive strength of the SPH-ECC was considered explicitly in the

Specimen	Load carrying capacity		
	$P_{\text{Max-Test}}$ (kN)	$P_{\text{Max-FEM}}$ (kN)	$P_{\text{Max-FEM}}/P_{\text{Max-Test}}$
CB	168.5	169.5	1.00
SB-2	310.0	307.1	0.99
SB-3	354.0	351.7	0.99
Mean			0.99

TABLE 6 Comparison of experimental and FEM results.

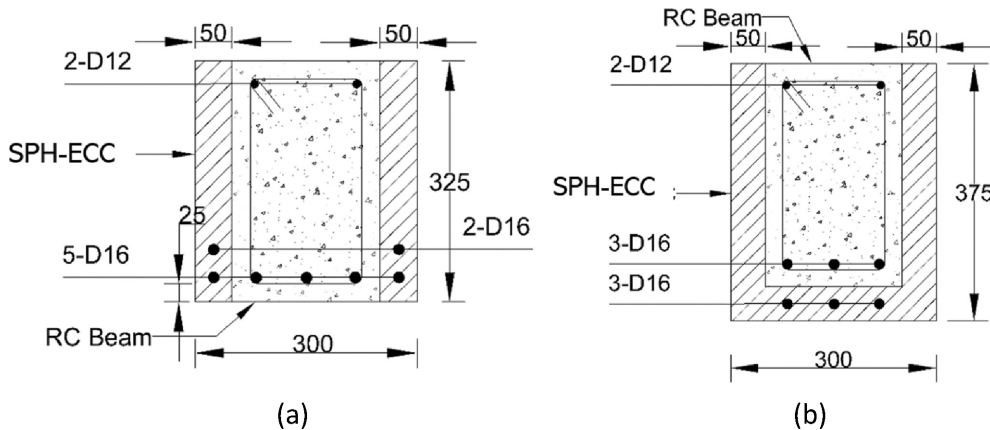


FIGURE 6 Cross-sectional details of (a) model SB-2/N4D16 and (b) model SB-3/N3D16.

parametric study, the tensile strength of the SPH-ECC was not explicitly considered as a design parameter. This was because in the previous experimental study,¹ the failure mode of both the SB-2 and SB-3 beams was the crushing of the top SPH-ECC layer. Hence, it was suspected that the compressive strength might significantly affect the performance of the strengthen beams. Furthermore, for the SB-2 beam, the area of SPH-ECC under compression was only slightly larger than the area under tension,¹ while for the SB-3 beam the area of SPH-ECC under tension is roughly 2.5–3 times larger than that under compression. However, the compressive strength of SPH-ECC (50 MPa to 75 MPa, Table 4) is at least 10 times higher than the tensile strength (5 MPa, Table 5). Hence, together with the fact that the ultimate strength of the beams was controlled by crushing of top SPH-ECC/concrete layers, it is expected that the effect of the tensile strength on the performance of the beams would be less than that of the compression strength.

It should also be noted that the tensile strength of SPH-ECC had *actually* been considered *implicitly* in the parametric study by varying the compressive strength of the SPH-ECC (Table 5). As mentioned in Section 2.2, the tensile strength of SPH-ECC is not an independent property (i.e., one simply cannot freely change the tensile strength of SPH-ECC without changing its compressive strength). Since during the mix design of most ECC, the target compressive strength is normally selected as the primary design parameter, it was

selected as one of the explicit parameters while the SPH-ECC tensile strength was only considered implicitly in this study.

Based on practical consideration and the minimum cover thickness required for reinforcement bars, thickness of side SPH-ECC layers of SB-2 configuration and bottom SPH-ECC layer of SB-3 configuration was kept as a constant of 50 mm. Thus, the effect of SPH-ECC layer thickness was studied only for the SB-3 configuration by varying the thickness of the side SPH-ECC layers from 50 mm to 30 mm.

For the area of reinforcement bars embedded in SPH-ECC layer(s), since the cross-sectional geometries of SB-2 and SB-3 configurations are different (Figure 2b,c), their arrangements of embedded reinforcement bars are also different. For the SB-2 configuration, either one layer (Figure 2b) or two layers (Figure 6a) of $\varnothing 16$ reinforcement bars were placed in each side SPH-ECC layer which resulted in either two reinforcement bars (Figure 2b, area = 401.92 mm²) or four reinforcement bars (Figure 6a, area = 803.84 mm²) in the SPH-ECC layers. On the other hand, for the SB-3 configuration, either two $\varnothing 16$ reinforcement bars (Figure 2c, area = 401.92 mm²) or three $\varnothing 16$ reinforcement bars (Figure 6b, area = 602.88 mm²) were placed in the bottom SPH-ECC layer in the models. It should be noted that due to cover thickness requirement, variation of reinforcement ratio was achieved by varying the number of reinforcement bars used rather than increasing the bar diameter.

TABLE 7 Details of models used in parametric study.

Model ID	Material properties		Geometric properties	
	Concrete compressive strength, f_c (MPa)	SPH-ECC compressive strength, f_{Ec} (MPa)	SPH-ECC side layers thickness, t_{Es} (mm)	Area of reinforcement bars in SPH-ECC layers, A_{Es} (mm ²)
SB-2/C30E70T50N2D16^a	30	70	50	401.92
SB-2/C30E70T50N4D16				803.84
SB-2/C30E50T50N2D16		50		401.92
SB-2/C30E50T50N4D16				803.84
SB-2/C45E70T50N2D16	45	70		401.92
SB-2/C45E70T50N4D16				803.84
SB-2/C45E50T50N2D16		50		401.92
SB-2/C45E50T50N4D16				803.84
SB-3/C30E75T50N2D16^a	30	75	50	401.92
SB-3/C30E75T30N2D16			30	
SB-3/C30E75T50N3D16			50	602.88
SB-3/C30E75T30N3D16			30	
SB-3/C30E50T50N2D16		50	50	401.92
SB-3/C30E50T30N2D16			30	
SB-3/C30E50T50N3D16			50	602.88
SB-3/C30E50T30N3D16			30	
SB-3/C45E75T50N2D16	45	75	50	401.92
SB-3/C45E75T30N2D16			30	
SB-3/C45E75T50N3D16			50	602.88
SB-3/C45E75T30N3D16			30	
SB-3/C45E50T50N2D16		50	50	401.92
SB-3/C45E50T30N2D16			30	
SB-3/C45E50T50N3D16			50	602.88
SB-3/C45E50T30N3D16			30	

^aBaseline models corresponding to specimens tested in Reference 1.

The two specimens tested in the previous study¹ were adopted as baseline models for the numerical parametric study. Based on these two baseline models and the above choices of values of key parameters, 8 and 16 different strengthened beam models were created for the SB-2 configuration and the SB-3 configuration, respectively. Details of these 24 models used are summarized in Table 7. For each created model listed in Table 7, a model ID was assigned. These model IDs start with the strengthening configuration (SB-2 and SB-3) and then followed by the material and geometric properties considered in the numerical parametric study. Full description of the abbreviations used in the model ID are provided in Table 8. It should be noted that the models SB-2/C30E70T50N2D16 and SB-3/C30E75T50N2D16 are corresponding to the SB-2 and SB-3 strengthened beams tested in Reference 1,

respectively. It should be noted that all these 32 beams modeled were designed to be under-reinforced in the sense that the bottom reinforcement bars inside the SPH-ECC layers would be yielded first before the top concrete/SPH-ECC layer failed by compression.

3.2 | Numerical parametric study results

3.2.1 | General results

From the numerical parametric study results, it was found that all the modeled beams shown in Table 7 were failed by concrete/ECC crushing. These results confirmed that all beams were under-reinforced even after strengthening. In addition, it was found that similar to the

TABLE 8 Abbreviations used in Model ID.

Abbreviation	Description
SB	Strengthening configuration
C	Concrete compressive strength
E	SPH-ECC compressive strength
T	Thickness of sides SPH-ECC layers
N	Number of reinforcement bars in SPH-ECC
D	Diameter of reinforcement bars in SPH-ECC

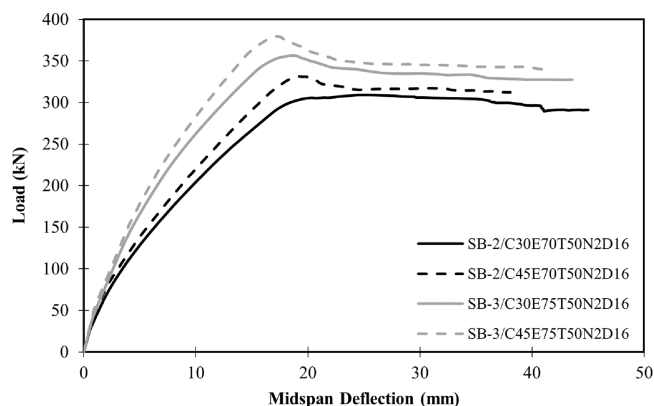


FIGURE 7 Load-deflection curves for models with different concrete compressive strengths.

experimental results,¹ there were significant increases in the initial stiffness for all the strengthened beams when compared with the original RC beam. Furthermore, detailed analysis of the numerical parametric study results also confirmed that the bond stress between the concrete and SPH-ECC interfaces for all modeled beams were well below the bond strength limit.¹¹ Hence, the use of the tie model in lieu of the more expensive cohesive element model was justified.

3.2.2 | Effect of concrete compressive strength

Figure 7 shows the load-deflection curves for models with concrete compressive strength varied from 30 MPa to 45 MPa with both types of strengthening configuration (SB-2 and SB-3) considered. The corresponding load capacities are summarized in Table 9. In these models, the side SPH-ECC layers thickness and the area of reinforcement bars were kept constant. It can be seen from Figure 7 and Table 9 that as the concrete compressive strength was increased from 30 to 45 MPa, for both types of strengthening configurations, the load carrying capacity was approximately increased by 8%. Hence, by

increasing the concrete compressive strength for 50%, only a marginal flexural strength enhancement was observed. The main reason for such a result was that as the strengthened beams were under-reinforced, the top concrete and SPH-ECC would only reach the peak compressive strength after the yielding of bottom reinforcement bars. As a result, the maximum load carrying capacity was largely determined by the reinforcement bar contributions and was not significantly changed by increasing the peak compressive strength of the concrete.

3.2.3 | Effect of SPH-ECC compressive strength

The effect of compressive strength of SPH-ECC was investigated by changing the compressive strength from 70 MPa to 50 MPa for the SB-2 configuration and 75 MPa to 50 MPa for the SB-3 configuration. The concrete compressive strength and SPH-ECC side layers thickness were fixed while different reinforcement bars were considered. Figure 8 shows the load-deflection curves obtained while the maximum load capacities obtained are summarized in Table 10. It can be seen from Figure 8 that the effect of SPH-ECC compressive strength was negligible. Table 10 also shows that even the SPH-ECC compressive strength was reduced by up to 33%, only 1.5%–2% of loading capacity reduction were observed for both types of strengthening configurations. Detailed analysis of the modeling results shown that in these models, immediately after the bottom reinforcement bars in the RC beam part and SPH-ECC layers were yielded, the compressive strain at the top surface reached was in the range of 0.001–0.002. Table 11 shows that the corresponding compressive stress in SPH-ECC at these strains (calculated by using Equation 3) was only slightly affected by the SPH-ECC grade. As the width (50 mm at most) of the top side SPH-ECC layers was relatively small compared with the width of the whole beam (300 mm), such a small change in compressive stress eventually resulted in a small change of the flexural strength. In addition, by comparing Figures 7 and 8, it can also be concluded that flexural behavior of strengthened beams is more sensitive to compressive strength of concrete than that of SPH-ECC.

3.2.4 | Effect of thickness of side SPH-ECC layers in SB-3

Since sufficient cover was required for reinforcement bars in the side SPH-ECC layers of SB-2 beam (Figure 2b) and bottom SPH-ECC layer of SB-3 beam (Figure 2c), the effect

TABLE 9 Effects of compressive strength of concrete.

Model ID	Material properties		Geometric properties		Load capacity (kN)
	f_c (MPa)	f_{Ec} (MPa)	t_{Es} (mm)	A_{Es} (mm ²)	
SB-2/C30E70T50N2D16	30	70	50	401.92	307.1
SB-2/C45E70T50N2D16	45				331.4
SB-3/C30E75T50N2D16	30	75			351.7
SB-3/C45E75T50N2D16	45				379.8

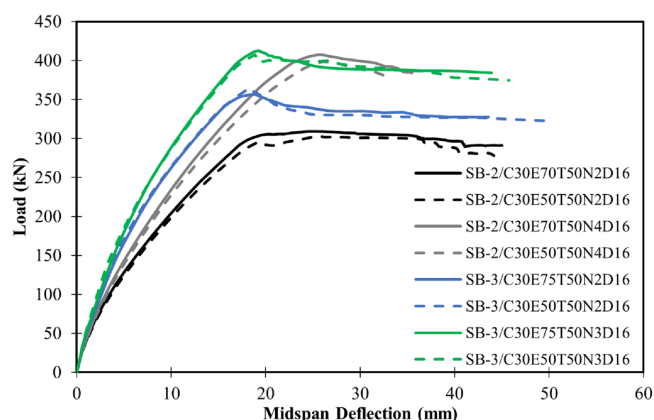


FIGURE 8 Load-deflection curves for models with different SPH-ECC compressive strengths.

of SPH-ECC layer thickness was only investigated by varying the thickness of side SPH-ECC layers of SB-3 beams from 50 mm to 30 mm. Figure 9 shows the effect of side SPH-ECC layers thickness while maximum load capacities are summarized in Table 12. Both concrete compressive strengths (30 MPa and 45 MPa) and area of reinforcement bars (401.92 mm² and 602.88 mm²) in the bottom SPH-ECC layer were considered by fixing the compressive strength of SPH-ECC to 75 MPa. Table 12 shows that by decreasing the side SPH-ECC layers thickness from 50 mm to 30 mm, the flexural strength was slightly decreased within a range of 3%–7%. Again, this was due to the fact that the beams are under-reinforced and the relatively small areas of the side SHP-ECC layers.

3.2.5 | Effect of reinforcement bars area in SPH-ECC layers

Figure 10 shows the effect of area of reinforcement bar in SPH-ECC layers on the flexural behavior of beams with both types of strengthening configurations. Table 13 summarizes the maximum load capacities obtained by changing the reinforcement bars area. Both concrete compressive strengths (30 MPa and 45 MPa) were considered by fixing the side SPH-ECC layers thickness at

50 mm and compressive strength of SPH-ECC to 70 MPa for SB-2 configuration and 75 MPa for SB-3 configuration. Table 13 and Figure 10 show that for both the SB-2 and SB-3 configurations, when compared the effects of concrete and SPH-ECC compressive strengths and SPH-ECC thickness, a much higher relative increase (28%–32%) in flexural capacities was observed by increasing reinforcement bars area. Such increase was more prominent for SB-2 beams as the number of bars embedded in the side SPH-ECC layers were double from 2 bars to 4 bars while for the SB-3 configuration, only one addition bar was added to the bottom SPH-ECC layer. This is expected as all beams are still under-reinforced after strengthening, increasing the reinforcement bar area could increase the flexural strength of the beams.

4 | ANALYTICAL MODELS FOR STRENGTHENED BEAMS

In this section, two analytical models are developed to predict the flexural strength of SPH-ECC strengthened beams for the SB-2 and SB-3 configurations. The main role of these analytical models is to provide a quick running tool allowing design engineers to quickly predict the flexural strength of the strengthened beams without running any FE models which is deemed to be too time consuming for day-to-day design work. It should be noted that in order to come up with these simple and easy to use analytical models, some simplified assumptions (given in Section 4.1.) are adopted and they may slightly reduce the accuracy of the analytical models when comparing with the detailed FE modeling results. Hence, it is important that the reliability and the accuracy of the suggested analytical should be verified against the parametric modeling results (Section 4.3).

4.1 | Assumptions used for the analytical models

The analytical models developed for both strengthened configurations are based on the following assumptions:

TABLE 10 Effects of compressive strength of SPH-ECC.

Model ID	Material properties		Geometric properties		
	f_c (MPa)	f_{Ec} (MPa)	t_{Es} (mm)	A_{Es} (mm ²)	Load capacity (kN)
SB-2/C30E70T50N2D16	30	70	50	401.92	307.1
SB-2/C30E50T50N2D16		50			302.4
SB-2/C30E70T50N4D16		70		803.84	407.5
SB-2/C30E50T50N4D16		50			398.6
SB-3/C30E75T50N2D16		75		401.92	351.7
SB-3/C30E50T50N2D16		50			344.7
SB-3/C30E75T50N3D16		75		602.88	412.5
SB-3/C30E50T50N3D16		50			407.2

TABLE 11 Compressive stress in SPH-ECC at 0.001 and 0.002 strain levels.

NC strength of SPH-ECC (MPa)	Stress (MPa) at 0.001 strain	Stress (MPa) at 0.002 strain
50	16.5	30.0
70	20.4	37.3
75	20.8	38.3

1. Strain distribution throughout the depth of the beam is linear and plane sections will remain plane and perpendicular to the neutral axis before and after bending.
2. Concrete tensile strength is neglected. This assumption was adopted to simplify the model because concrete provides very limited resistance under tension before and after cracks are formed.
3. Full composite action (i.e., no bond slip) with perfect interfacial bond are considered between SPH-ECC and concrete surfaces as well as embedded reinforcement bars. This assumption was adopted as in all tested beams¹ and parametric study models (Section 3), no bond slip was observed.
4. The compressive stresses distribution in concrete and side SPH-ECC layers is simplified as rectangular blocks having respectively uniform values of $0.85f_c$ and $0.85f_{Ec}$ over a depth 'a' (Figure 11) from the top surface of the beam. Note that by using this assumption in lieu of the more realistic linear varying stress distribution, the calculation steps of the analytical models are greatly simplified.
5. Tensile strength of SPH-ECC will be considered and assumed to be uniform throughout the bottom layer in the SB-3 configuration. While for the SB-2 configuration, tensile strength of SPH-ECC will be considered at bottom of each side layer in as a rectangular block with uniform stress value of f_{Et} over a height equal to 1.7

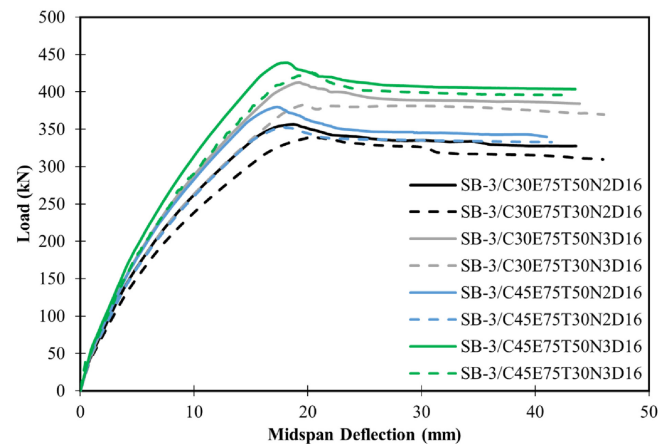


FIGURE 9 Load-deflection curves for SB-3 configuration models with different thicknesses of side SPH-ECC layers.

- times of layer thickness (Figure 11a,b). It should be noted that this assumption is largely based on the ECC strain analysis results obtained from the experimental study¹ and numerical parametric study (Section 3). It was found that for the SB-3 configuration, the bottom layer SPH-ECC provided most contribution. While for the SB-2 configuration, contribution of SPH-ECC above 1.7 times of the layer thickness is negligible.
6. All the embedded reinforcement bars in SPH-ECC layers will yield before reaching the maximum flexural capacity of the beams. Again, the use of this assumption was justified by the fact that in all experimental and numerical parametric study results, all strengthened beams showed a ductile, under-reinforced failure mode. However, in practical design, due care should be taken for this assumption by the design engineer to ensure that the strengthened beams should not be over-reinforced.

Based on the above assumptions, the internal forces and strain distributions of the strengthened beams are

TABLE 12 Effects of SPH-ECC layers thickness in SB-3 models.

Model ID	Material properties		Geometric properties		
	f_c (MPa)	f_{Ec} (MPa)	t_{Es} (mm)	A_{Es} (mm ²)	Load capacity (kN)
SB-3/C30E75T50N2D16	30	75	50	401.92	351.7
SB-3/C30E75T30N2D16			30		339.8
SB-3/C30E75T50N3D16			50		412.5
SB-3/C30E75T30N3D16			30		382.6
SB-3/C45E75T50N2D16	45	75	50	401.92	379.8
SB-3/C45E75T30N2D16			30		352.7
SB-3/C45E75T50N3D16			50		438.9
SB-3/C45E75T30N3D16			30		425.7

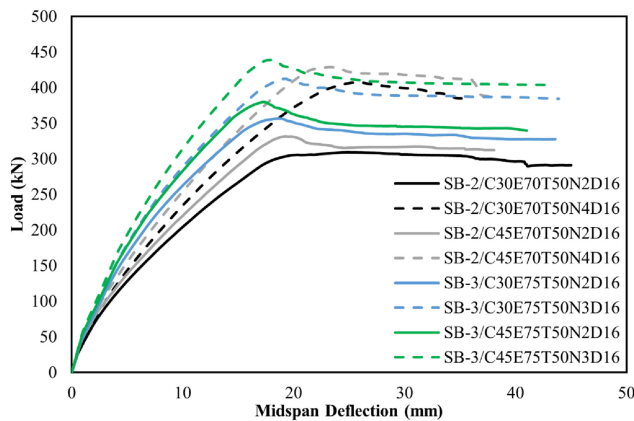


FIGURE 10 Load-deflection curves for models with different reinforcement bars area in SPH-ECC layers.

shown in Figure 11a,b for the SB-2 configuration with one and two layers of reinforcement bars, respectively. Force and strain distributions for the SB-3 configuration are shown in Figure 11c.

4.2 | Estimation of load-carrying capacities of strengthened beam

In order to estimate the maximum load carrying capacity, the first step is to assume the position of neutral axis (P.N.A.) from the top surface of the beam section. The moment capacity of the section can then be calculated by considering the forces and strain distributions shown in Figure 11 and the formulae given in Table 14. The whole calculated procedure is summarized as a flow chart shown in Figure 12. Notations used in Figures 11 and 12 and Table 14 are listed in Table 15. Note that based on the assumption (6) in Section 4.1, when the section reaches its flexural strength, values of ϵ_{Es1} and ϵ_{Es} in Figures 11 and 12 are expressed as

$$\epsilon_{Es1} = \epsilon_y = \frac{f_y}{E_s} \text{ and } \epsilon_{Es} = \alpha \frac{f_y}{E_s} \quad (7a)$$

where

$$\alpha = \begin{cases} 1 & \text{SB-2} \\ 1.1 & \text{SB-3} \end{cases} \quad (7b)$$

As shown in Equation (7b), a higher value of $\alpha = 1.1$ is used for the SB-3 configuration. It is due to the larger distance between the embedded reinforcement bars in the bottom SPH-ECC layer and the bottom reinforcement bars in the RC beam part which in general would not allow them to be yielded simultaneously. In fact, it is assumed that when the embedded reinforcement bars in the SPH-ECC layer have just yielded, the bottom reinforcement bars of RC beam part would still remain elastic. Therefore, a higher value of $\epsilon_{Es} = 1.1 \frac{f_y}{E_s}$ is used in the SB-3 configuration to allow a higher strain to be attained in the reinforcement bars embedded in the bottom SPH-ECC layer. This would ensure that reinforcement bars in the RC beam part would also be yielded at the peak load.

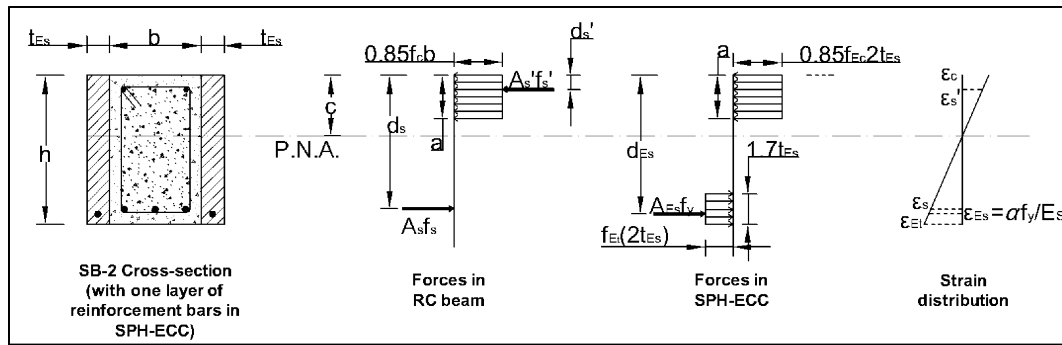
After the flexural strength of the strengthen section M_n is calculated, the maximum load capacity of the strengthened beams can be calculated by considering the bending moment diagram of the beams. For the case that the beam is under four-point bending as shown in Figure 1, the maximum load carrying capacity of the beam P (in kN) can be obtained by:

$$M_n = \frac{PL}{6} \quad (8)$$

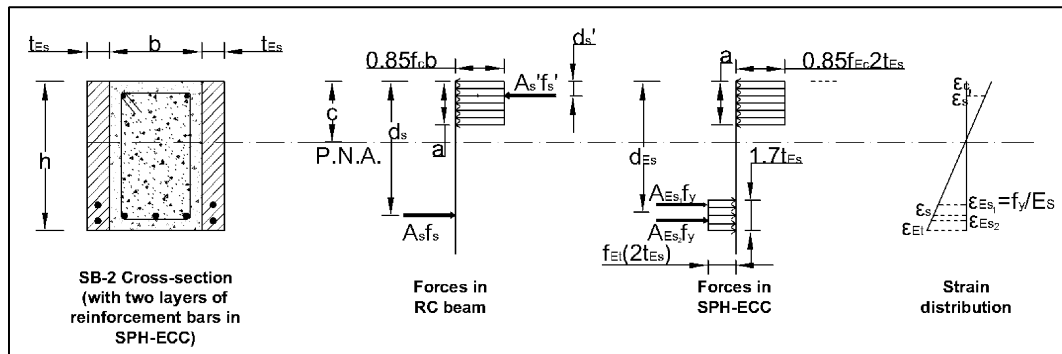
In Equation (8), L is clear span of beam between the supports (in meters). Obviously, the flexural loading capacity of a beam under other loading and support

TABLE 13 Effects of area of reinforcement bars in SPH-ECC layers.

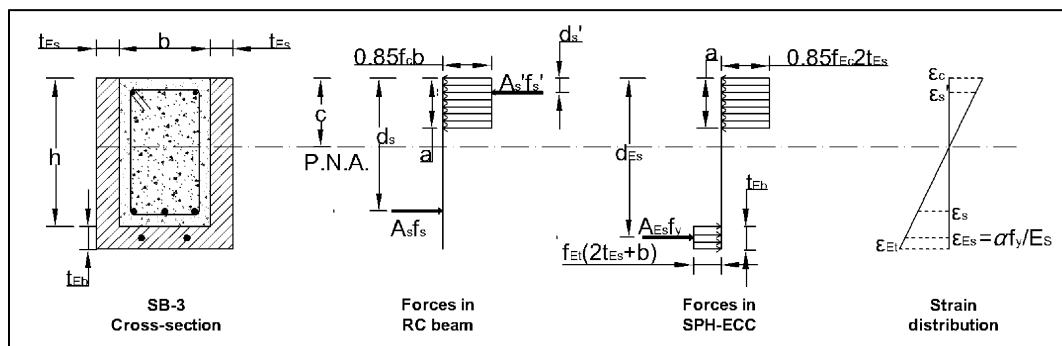
Model ID	Material properties		Geometric properties		Load capacity (kN)
	f_c (MPa)	f_{Ec} (MPa)	t_{Es} (mm)	A_{Es} (mm ²)	
SB-2/C30E70T50N2D16	30	70	50	401.92	307.1
SB-2/C30E70T50N4D16				803.84	407.5
SB-2/C45E70T50N2D16	45			401.92	331.4
SB-2/C45E70T50N4D16				803.84	427.6
SB-3/C30E75T50N2D16	30	75		401.92	351.7
SB-3/C30E75T50N3D16				602.88	412.5
SB-3/C45E75T50N2D16	45			401.92	379.8
SB-3/C45E75T50N3D16				602.88	438.9



(a)



(b)



(c)

FIGURE 11 Cross-section, forces and strain distributions of (a) SB-2 configuration with one layer of reinforcement bars, (b) SB-2 configuration with two layers of reinforcement bars, and (c) SB-3 configuration.

conditions can be obtained similarly by identifying the relationship between the maximum bending moment and the loading applied.

4.3 | Verification of the proposed analytical models

In order to validate the proposed analytical models, the maximum load capacities for the strengthened beam models used in the parametric numerical study are calculated through analytical model (P_{AN}) and compared with

the corresponding values predicted by the FEM model (P_{FEM}) for the SB-2 and SB-3 configurations in Tables 16 and 17, respectively. As shown in Tables 16 and 17, the differences between the analytical and numerical modeling results were within 2%–7% for the SB-2 configuration and 1%–9% for the SB-3 configuration. For both configurations, the analytical model generally slightly underestimated the loading capacity of the strengthened beam so they would be conservative and safe when used in practice. Furthermore, from the mean and standard deviation values of P_{AN}/P_{FEM} shown in Tables 16 and 17, it can be concluded that the proposed analytical models could

TABLE 14 Analytical expression for compressive stress rectangular block depths and nominal moment capacities.

Strengthening configuration	SB-2	SB-3
Compressive stress rectangular block depth	$a = \frac{A_{Es}f_y + A_s f_s + 3.4t_{Es}^2 f_{Et} - A_s' f_s'}{0.85(f_c b + 2f_{Ec} t_{Es})}$	$a = \frac{A_{Es}f_y + A_s f_s + (2t_{Es} + b)t_{Eb} f_{Et} - A_s' f_s'}{0.85(f_c b + 2f_{Ec} t_{Es})}$
Moment capacity by RC beam part, M_{n1}	$M_{n1} = A_s' f_s' (d - d') + (A_s f_s - A_s' f_s') (d - \frac{a}{2})$	$M_{n1} = A_s' f_s' (d - d') + (A_s f_s - A_s' f_s') (d - \frac{a}{2})$
Moment capacity by SPH-ECC layer part, M_{n2}	$M_{n2} = A_{Es} f_y (d_{Es} - \frac{a}{2}) + 3.4t_{Es}^2 f_{Et} (h - \frac{1.7t_{Es} + a}{2})$	$M_{n2} = A_{Es} f_y (d_{Es} - \frac{a}{2}) + f_{Et} t_{Eb} (2t_{Es} + b) (h - \frac{t_{Es} + a}{2})$

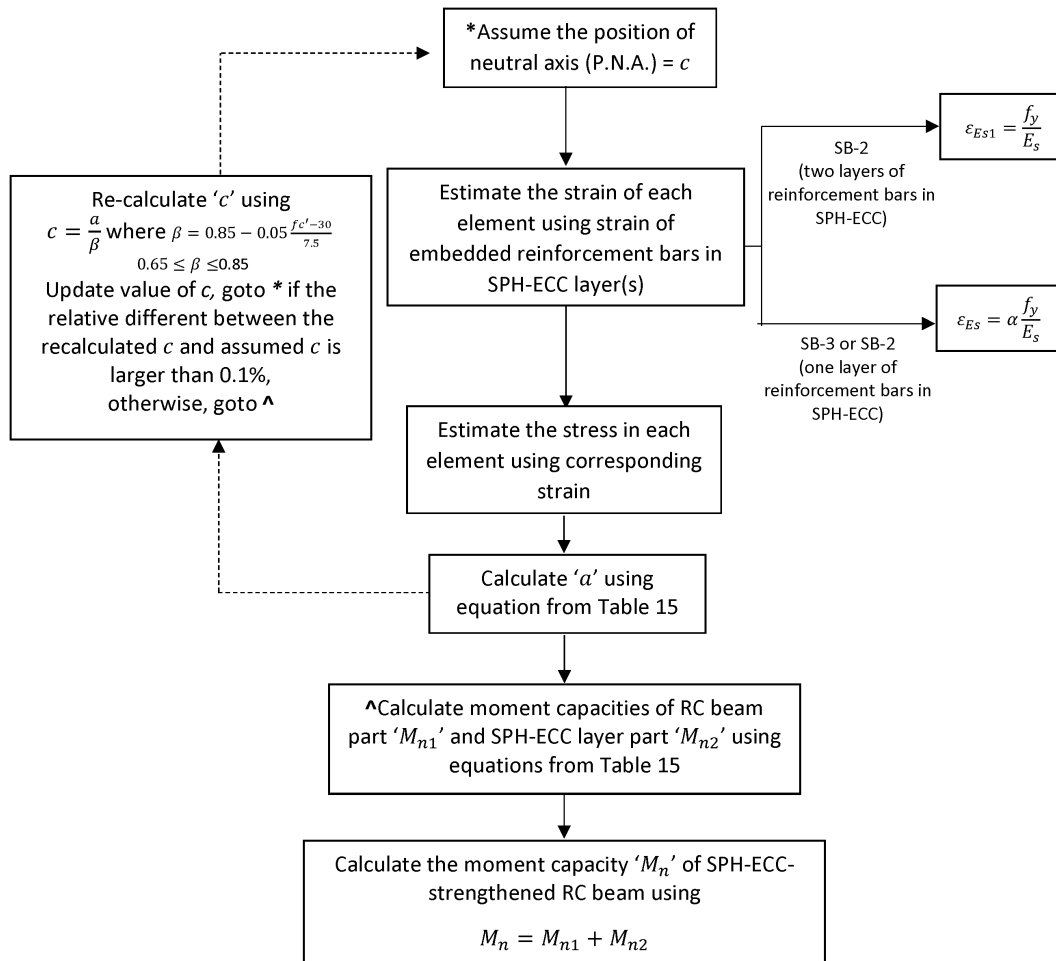


FIGURE 12 Flow chart for calculation of moment capacity of SPH-ECC strengthened RC beam.

TABLE 15 Notations used in Figures 11 and 12 and Table 14.

Notations	Definition
t_{Es}	Thickness of the side SPH-ECC layers in SB-2 and SB-3 configurations
t_{Eb}	Thickness of bottom SPH-ECC layer in SB-3 configuration
b	Width of RC beam part
h	Height of RC beam part
c	Depth of P.N.A. from top surface of the beam
d_s'	Effective depth of top reinforcement bars in RC beam part from top surface of beam
d_s	Effective depth of bottom reinforcement bars in RC beam part from top surface of beam
d_{Es}	Effective depth of reinforcement bars in SPH-ECC layer from top surface of beam
a	Depth of compressive stress rectangular block in concrete/side SPH-ECC layers from top surface of beam
A_s'	Area of top reinforcement bars in RC beam part
A_s	Area of bottom reinforcement bars in RC beam part
A_{Es}	Area of reinforcement bars in SPH-ECC layers of SB-3 (Figure 11c) or SB-2 when only one layer of reinforcement bars is used (Figure 11a)
A_{Es1}	Area of top layer reinforcement bar in side SPH-ECC layers of SB-2 when two layers of reinforcement bars are used (Figure 11b)
A_{Es2}	area of bottom layer reinforcement bars in side SPH-ECC layers of SB-2 when two layers of reinforcement bars are used (Figure 11b)
ϵ_{Et}	Strain in SPH-ECC layer at bottom surface of beam
ϵ_c	Strain at top concrete surface of the beam
ϵ_s'	Strain in top reinforcement bars in RC beam part
ϵ_s	Strain in bottom reinforcement bars in RC beam part
ϵ_{Es}	Strain in reinforcement bars in bottom SPH-ECC layer of SB-3 or SB-2 when only one layer of reinforcement bars is used (Figure 11a)
ϵ_{Es1}	Strain in top reinforcement bar layer in side SPH-ECC layer of SB-2 when two layers of reinforcement bars are used (Figure 11b)
ϵ_{Es2}	Strain in bottom layer of reinforcement bars in side SPH-ECC layers of SB-2 when two layers of reinforcement bars are used (Figure 11b)
E_s	Modulus of elasticity for reinforcement bars
f_y	Yielding strength of reinforcement bars
M_{n1}	Moment capacity of the RC beam part
M_{n2}	Moment capacity of the SPH-ECC part
M_n	Moment capacity of the strengthen section

TABLE 16 Comparison of analytical and numerical modeling results of SB-2 beams.

Model ID	Load capacity form FEM (kN), P_{FEM}	Load capacity from analytical model, P_{AN}	P_{AN}/P_{FEM}
SB-2/C30E70T50N2D16	307.1	300.9	0.98
SB-2/C30E70T50N4D16	407.5	378.6	0.93
SB-2/C30E50T50N2D16	302.4	286.9	0.95
SB-2/C30E50T50N4D16	398.6	376.9	0.95
SB-2/C45E70T50N2D16	331.4	310.2	0.94
SB-2/C45E70T50N4D16	427.6	395.9	0.93
SB-2/C45E50T50N2D16	323.0	307.1	0.95
SB-2/C45E50T50N4D16	420.3	397.0	0.94
Mean			0.95
SD			0.016

TABLE 17 Comparison of analytical and numerical modeling results of SB-3 beams.

Model ID	Load capacity from FEM (kN), P_{FEM}	Load capacity from analytical model, P_{AN}	P_{AN}/P_{FEM}
SB-3/C30E75T50N2D16	351.4	339.3	0.97
SB-3/C30E75T30N2D16	339.8	325.8	0.96
SB-3/C30E75T50N3D16	412.5	404.3	0.98
SB-3/C30E75T30N3D16	382.6	389.3	1.02
SB-3/C30E50T50N2D16	344.7	325.7	0.95
SB-3/C30E50T30N2D16	327.6	314.6	0.96
SB-3/C30E50T50N3D16	407.2	389.8	0.96
SB-3/C30E50T30N3D16	382.4	377.3	0.99
SB-3/C45E75T50N2D16	379.8	346.0	0.91
SB-3/C45E75T30N2D16	352.7	333.9	0.95
SB-3/C45E75T50N3D16	438.9	413.2	0.94
SB-3/C45E75T30N3D16	425.7	400.2	0.94
SB-3/C45E50T50N2D16	355.8	333.0	0.94
SB-3/C45E50T30N2D16	352.0	323.2	0.92
SB-3/C45E50T50N3D16	428.5	399.3	0.93
SB-3/C45E50T30N3D16	410.4	389.3	0.95
Mean			0.95
SD			0.027

predict the flexural strength of SPH-ECC strengthened RC beams with 92%–98% of accuracy.

5 | CONCLUSION

This study presented the results of a numerical parametric study on two different strengthening configurations (SB-2 configuration and SB-3 configuration) for reinforced concrete (RC) beams using steel and polyvinyl-alcohol hybrid fiber reinforced engineered cementitious composite (SPH-ECC) with embedded reinforcement bars. Influences of four key design parameters on the flexural behavior of beams were studied. Two simple and easy to use analytical models were also developed to predict the flexural strength of beams for these two types of strengthening configurations. The main functions of the parametric study are (i) to obtain some crucial insights and data on the general flexural behaviors of the strengthened beams and facilitate the development of the analytical models and (ii) to validate the accuracy and reliability of the analytical models. Based on the findings of this research, following conclusions could be drawn.

1. The use of tie model to define interfacial bond behavior between SPH-ECC and concrete could

accurately predict the flexural response of SPH-ECC strengthened RC beams for both strengthening configurations.

2. The flexural strength of strengthened beam is only slightly affected by the compressive strength of concrete used. While for the SPH-ECC compressive strength and the thickness of side SPH-ECC layers, provided that reasonable values are used (e.g., satisfies the maximum reinforcement bars cover thickness requirement and with comparable strength with the concrete strength), their effects are negligible.
3. It was noticed that for both types of strengthening configurations, among all the parameters studied, the area of reinforcement bars embedded in SPH-ECC layers produced the biggest effects on the flexural strength.
4. In term of flexural strength enhancement and cost-effectiveness, it was found that generally the SB-3 strengthening configuration could provide more strength enhancement than the SB-2 configuration by using a similar number of rebars used and a small additional amount of SPH-ECC materials. However, in practice, it should be mentioned that constraints in headroom requirement may impose a stringent limit on the total beam depth. In such situation, the SB-2 configuration will be the only feasible option. Of course, if headroom requirement is not a concern, the

SB-3 configuration is the preferred option in term of strength enhancement.

- The proposed simple and easy to use analytical models for the two strengthening configurations could provide accurate predictions of the flexural strength of the strengthened beams.

Finally, it should be mentioned that while the proposed analytical models could provide quick and accurate predictions for the loading capacity of the strengthened beams, a larger scale parametric investigation is required to develop more reliable and comprehensive analytical models that could trace out the complete load–deflection curves of the strengthened RC beam up to failure, and this could be an important potential future research topic.

ACKNOWLEDGMENTS

UNSW Canberra's support for the first author for this research through Tuition Fee Scholarship is gratefully acknowledged. Open access publishing facilitated by University of New South Wales, as part of the Wiley - University of New South Wales agreement via the Council of Australian University Librarians.

DATA AVAILABILITY STATEMENT

The data that support the findings of this study are available from the corresponding author upon reasonable request.

ORCID

C. K. Lee  <https://orcid.org/0000-0001-8342-6442>

REFERENCES

- Qasim M, Lee CK, Zhang YX. Flexural strengthening of reinforced concrete beams using hybrid fibre reinforced engineered cementitious composite. *Eng Struct*. 2023;284:115992.
- Shang X-Y, Yu J-T, Li L-Z, Lu Z-D. Strengthening of RC structures by using engineered cementitious composites: a review. *Sustainability*. 2019;11(12):18.
- Li VC, Wang S, Wu C. Tensile strain-hardening behavior of polyvinyl alcohol engineered cementitious composite (PVA-ECC). *ACI Mater J*. 2001;98(6):10.
- Kim YY, Lee BY, Bang JW, Han B-C, Feo L, Cho C-G. Flexural performance of reinforced concrete beams strengthened with strain-hardening cementitious composite and high strength reinforcing steel bar. *Composites: Part B*. 2014;56:8–519.
- Wu C, Li VC. CFRP-ECC hybrid for strengthening of the concrete structures. *Compos Struct*. 2017;178:11–382.
- Pourfalah S. Behaviour of engineered cementitious composites and hybrid engineered cementitious composites at high temperatures. *Construct Build Mater*. 2018;158:921–37.
- Lai BL, Zhang MY, Zheng XF, Chen ZP, Zheng YY. Experimental study on the axial compressive behaviour of steel reinforced concrete composite columns with stay-in-place ECC jacket. *J Build Eng*. 2023;68:106174.

- Deng M, Zhang Y, Li Q. Shear strengthening of RC short columns with ECC jacket: cyclic behavior tests. *Eng Struct*. 2018; 160:11–545.
- Hung CC, Chen YS. Innovative ECC jacketing for retrofitting shear-deficient RC members. *Construct Build Mater*. 2016;111: 11–418.
- Yang X, Gao WY, Dai JG, Lu ZD, Yu KQ. Flexural strengthening of RC beams with CFRP grid-reinforced ECC matrix. *Compos Struct*. 2018;189:18–26.
- Qasim M, Lee CK, Zhang YX. An experimental study on interfacial bond strength between hybrid engineered cementitious composite and concrete. *Construct Build Mater*. 2022;356:129299.
- Tinoco MP, Silva FA. Repair of pre-damaged RC beams using hybrid fiber reinforced strain hardening cementitious composites. *Eng Struct*. 2021;235:112081.
- Khalil AE-H, Etman E, Atta A, Essam M. Nonlinear behavior of RC beams strengthened with strain hardening cementitious composites subjected to monotonic and cyclic loads. *Alex Eng J*. 2016;55:14–1496.
- Khan MKI, Lee CK, Zhang YX. Parametric study on high strength ECC-CES composite columns under axial compression. *J Build Eng*. 2021;44:102883.
- Khan MKI, Lee CK, Zhang YX. Numerical modelling of engineered cementitious composites-concrete encased steel composite columns. *J Constr Steel Res*. 2020;170:106082.
- Abaqus/CAE user's manual. Rhode Island: Dassault Systemes-Simulia Corp. 2014.
- Al-Osta MA, Isa MN, Baluch MH, Rahman MK. Flexural behavior of reinforced concrete beams strengthened with ultra-high performance fiber reinforced concrete. *Construct Build Mater*. 2017;134:18–296.
- Carreira D, Chu K. Stress–strain relationship for plain concrete in compression. *ACI J*. 1985;82:797–804.
- Hassan MK. Behaviour of hybrid stainless-carbon steel composite beam-column joints. Australia: Doctoral, Western Sydney University; 2016.

AUTHOR BIOGRAPHIES



M. Qasim, School of Engineering and Technology, University of New South Wales, Canberra, NSW, Australia.
Email: civil.qasim@gmail.com



Y. X. Zhang, School of Engineering, Design and Built Environment, Urban Transformations Research Centre, Western Sydney University, Penrith, NSW, Australia.
Email: Sarah.Zhang@westernsydney.edu.au



C. K. Lee, School of Engineering and Technology, University of New South Wales, Canberra, NSW, Australia.
Email: c.lee@adfa.edu.au

How to cite this article: Qasim M, Zhang YX, Lee CK. Numerical and analytical modeling of SPH-ECC strengthened RC beams. *Structural Concrete*. 2024;25(2):1129–47. <https://doi.org/10.1002/suco.202300407>